The dual role of martensitic transformation in fatigue crack growth

Xiaogang Wang[a], Chenghuan Liu[a], Binhan Sun[b,1], Dirk Ponge[b], Chao Jiang[a,1], and Dierk Raabe[b]

[a]State Key Laboratory of Advanced Design and Manufacturing for Vehicle Body, College of Mechanical and Vehicle Engineering, Hunan University, 410082 Changsha, China; and [b]Department of Microstructure Physics and Alloy Design, Max-Planck-Institut für Eisenforschung GmbH, 40237 Düsseldorf, Germany

Edited by Yonggang Huang, Northwestern University, Glencoe, IL; received June 1, 2021; accepted January 18, 2022

Deformation-induced martensitic transformation (DIMT) has been used for designing high-performance alloys to prevent structural failure under static loads. Its effectiveness against fatigue, however, is unclear. This limits the application of DIMT for parts that are exposed to variable loads, although such scenarios are the rule and not the exception for structural failure. Here we reveal the dual role of DIMT in fatigue crack growth through in situ observations. Two antagonistic fatigue mechanisms mediated by DIMT are identified, namely, transformation-mediated crack arresting, which prevents crack growth, and transformation-mediated crack coalescence, which promotes crack growth. Both mechanisms are due to the hardness and brittleness of martensite as a transformation product, rather than to the actual transformation process itself. In fatigue crack growth, the prevalence of one mechanism over the other critically depends on the crack size and the mechanical stability of the parent austenite phase. Elucidating the two mechanisms and their interplay allows for the microstructure design and safe use of metastable alloys that experience fatigue loads. The findings also generally reveal how metastable alloy microstructures must be designed for materials to be fatigue-resistant.

martensitic transformation | fatigue | structural failure | metastable alloy

Deformation-induced martensitic transformation (DIMT) (1, 2) has been used as an effective strengthening mechanism to design strong and ductile alloys for engineering applications. For instance, the use of the transformation-induced plasticity (TRIP) effect (3, 4) to overcome the strength–ductility trade-off (5) has enabled many high-performance alloys, such as advanced steels (6, 7), titanium alloys (8), and high-entropy alloys (9). Yet, such design concepts are based on the assumption of flaw-free alloys subjected to static loads. However, the damage tolerance of real engineering materials critically depends on their resistance to small flaws under variable loading conditions (10–12), which, if not properly considered, may lead to unexpected fatigue failure and catastrophic accidents. In this regard, a comprehensive understanding of the role of DIMT in fatigue crack growth is still missing. This limits the application of DIMT in many key engineered systems requiring high fatigue reliability, such as trains, airplanes, spacecraft, and power plants.

The complexity of this topic is reflected by the many mechanisms (13–15) that have been proposed so far on the possible influence of DIMT on fatigue crack growth. A recognized beneficial effect of DIMT is transformation-induced crack closure (TICC) (16). It is conventionally understood as a kind of crack closure similar to the classic plasticity-induced crack closure (17), in which the TRIP effect effectively contributes to the residual tensile deformation that is remaining in the crack wake. This gives rise to premature contact between the crack faces and results in a reduction in the effective crack driving force. Detailed theoretical and experimental studies (18–21) have revealed another main reason for this effect. It is the compressive residual stress generated by DIMT at the crack tip, which can locally compensate the far-field tensile stress. Another common explanation for crack retardation suggests that the occurrence of DIMT at the crack tip absorbs strain energy that would otherwise be available for crack growth. This effect is referred to as transformation-induced energy absorption (TIEA) (22, 23). It has also been shown that the DIMT can lead to crack path deflection, an effect referred to as transformation-induced crack deflection (TICD) (21, 24, 25). This mechanism leads to a zigzag crack path, which decelerates crack growth compared to a flat path (26). In addition, it can also increase the roughness level of crack surfaces, which in turn contributes to roughness-induced crack closure (RICC) (14, 27). In contrast to these effects that can reduce the crack growth rate, other studies (28, 29) have shown detrimental effects of DIMT. One of the main concerns is the brittleness of the fresh martensite that is formed as a transformation product at the crack tip (14, 21). This effect reduces the fracture toughness of the material (22), as brittle martensite is liable to crack initiation (18, 30). In this work, we investigate the effect of DIMT on fatigue crack growth in a model medium-Mn TRIP steel by conducting in situ fatigue tests in a scanning electron microscope (SEM). This allows capturing the detailed crack growth process and its interactions with the evolving microstructure. The study demonstrates both the beneficial and adverse effects of DIMT on fatigue crack growth. An unexpected finding is that these effects do not depend on the transformation process itself but on the characteristics of the transformation product, i.e., the hard and brittle martensite. They also show a strong

Significance

About 90% of all mechanical service failures are caused by fatigue. Avoiding fatigue failure requires addressing the wide knowledge gap regarding the micromechanical processes governing damage under cyclic loading, which may be fundamentally different from that under static loading. This is particularly true for deformation-induced martensitic transformation (DIMT), one of the most common strengthening mechanisms for alloys. Here, we identify two antagonistic mechanisms mediated by martensitic transformation during the fatigue process through in situ observations and demonstrate the dual role of DIMT in fatigue crack growth and its strong crack-size dependence. Our findings open up avenues for designing fatigue-resistant alloys through optimal use of DIMT. They also enable the development of physically based lifetime prediction models with higher fidelity.

Author contributions: X.W., B.S., C.J., and D.R. designed research; X.W., C.L., B.S., and D.P. performed research; X.W., C.L., and B.S. analyzed data; and X.W., B.S., and D.R. wrote the paper.

The authors declare no competing interest.

This article is a PNAS Direct Submission.

[1]To whom correspondence may be addressed. Email: b.sun@mpie.de or jiangc@hnu.edu.cn.

This article contains supporting information online at http://www.pnas.org/lookup/suppl/doi:10.1073/pnas.2110139119/-/DCSupplemental.

Published February 24, 2022.

dependence on the crack size and the mechanical stability of the host phase against transformation. These observations allow us to better understand and reconcile the sometimes contradictory fatigue phenomena that were reported for alloys with metastable phases. More specifically, we find that for different loading scenarios and alloy stabilities, different fatigue mechanisms can prevail during the different crack growth stages. These findings thus provide an in-depth understanding of the role of DIMT in fatigue crack growth. They also open up new pathways for designing fatigue-resistant alloys through optimal use of DIMT.

Results

Fatigue Testing under Variable DIMT Conditions. The material explored in this study is a medium-Mn dual-phase steel (0.2C-10Mn-3Al-1Si, in wt %) consisting of ferrite (α phase) and metastable austenite (γ phase). A unique feature of this alloy class is that it allows adjusting the volume fraction and mechanical stability of the host austenite phase over a wide range. The former parameter determines the maximum amount of DIMT and the latter controls the activation stress and the rate of martensite (α′ phase) formation as a function of strain (i.e., DIMT kinetics). These two factors jointly define the degree of DIMT. Here we test the material in two different microstructural conditions (i.e., two different microstructure variants). They were tailored using different intercritical annealing temperatures, which in turn produce different partitioning ratios of C and Mn. This creates austenite with different volume fractions and mechanical stability, as the partitioning produces different chemical driving force ($|\Delta G_{\gamma\rightarrow\alpha'}|$) for martensite formation (see *Materials and Methods* and *SI Appendix*, Fig. S1). One microstructure variant obtained has a high tendency to undergo DIMT (H-DIMT material, $|\Delta G_{\gamma\rightarrow\alpha'}|$ = 3,650 J/mol at room temperature, calculated by the Thermo-Calc software), producing a maximum of ∼65 vol % α′-martensite formation when mechanically loaded. Austenite-to-martensite transformation occurs immediately with the onset of plastic deformation. This leads to the formation of a phase transformation zone within the near-tip plastic zone of a propagating crack, as schematically shown in Fig. 1*A*. The size of the plastic zone increases with the stress intensity range ΔK, as confirmed by the full-field strain measurement using the microscopic digital image correlation (μ-DIC) method. We here define the size of the phase transformation zone (ω_T) as the distance perpendicular from the fatigue crack under which more than 90% of the initial austenite has transformed to martensite. The test sample of the H-DIMT material has a transformation zone size of 1.6 μm, 8.0 μm, and 20.7 μm under a stress intensity ΔK of 8.7 MPa $m^{1/2}$ (crack extension 20 μm), 14.0 MPa $m^{1/2}$ (crack extension 200 μm), and 30.7 MPa $m^{1/2}$ (crack extension 670 μm), respectively (Fig. 1*B*).

In contrast, the other microstructure variant has a lower fraction of austenite (∼30 vol %) and a higher mechanical stability of this phase. This leads to a low DIMT effect (L-DIMT material, $|\Delta G_{\gamma\rightarrow\alpha'}|$ = 3,276 J/mol at room temperature). For test samples of this material, DIMT occurs only when a fatigue crack passes through the host austenite phase (Fig. 1*C*). More specifically, we find that the transformation zone is confined to the one or two austenite grains that are closest to the crack tip (below 1 μm). It is also important to note that the transformation zone does not alter with ΔK within the range that has been probed (up to 34 MPa $m^{1/2}$). The distinct difference in DIMT and the resulting difference in the size of the near-tip transformation zone between the two types of materials enable a critical assessment of the influence of DIMT on fatigue crack growth.

We performed fatigue crack growth rate (FCGR) tests on samples of both types of materials under high-cycle fatigue testing conditions. A specially designed hydraulic fatigue testing system equipped with an SEM was used, which enabled in situ observation of microcrack growth in real time. Fig. 1*D* illustrates the measured crack growth rates da/dN as a function of ΔK within the range of applied stress and crack length (see *Materials and Methods*). It shows significant differences between the curves of the two types of materials with their different austenite stability. More specifically, the H-DIMT material with high austenite stability shows an up to two orders of magnitude lower crack growth rate than the L-DIMT material with low austenite stability (1.44×10^{-11} to 1.12×10^{-8} m per cycle vs. 1.39×10^{-9} to 1.12×10^{-8} m per cycle) at the short crack stage (denoted as Stage I, with a crack extension $\Delta a < 150$ μm). However, this situation is overturned at the long crack stage (denoted as Stage II, with a crack extension $\Delta a > 150$ μm), where the crack growth rate of the H-DIMT material is consistently higher than that of the L-DIMT material, namely, by up to five to seven times (1.12×10^{-8} to 5.09×10^{-7} m per cycle vs. 1.12×10^{-8} to 8.88×10^{-8} m per cycle). All comparisons are made under the same applied ΔK value, and the distinction of Stage I and Stage II is based on the relative relationship between the crack growth rates of the two materials being compared. In view of these essential differences in material behavior and their relation to the austenite stability, and the unexpected cross-over behavior between the short and the long crack regimes, we next analyze the DIMT accompanied fatigue crack growth and the associated microstructure changes in greater detail.

Fatigue Crack Arresting at Stage I. Concerning the short crack stage, the most striking finding is an abnormal crack growth retardation effect that is frequently observed in the H-DIMT material. The abnormality of this effect is reflected in its sudden appearance and persistence and its significant influence on the crack growth rate. It occurs when a crack tip encounters the phase boundary of a martensite grain in the direction along the crack path, as a typical example illustrated in Fig. 2. Fig. 2 *A* and *B* show that the fatigue crack propagated continuously when passing through an α-ferrite grain from N_1 to N_2 (containing 3,996 cycles). Then, the crack tip was suddenly blocked at the interface between the past α-ferrite grain and the forward α′-martensite grain. The α′-martensite grain was the product of DIMT from its parent γ-austenite phase, as confirmed by electron backscatter diffraction (EBSD) before and after the mechanical test (Fig. 2 *C* and *D*, respectively). Note that the near-tip transformation zone at the current crack length was about 2 μm. It was four times the average grain size of the parent austenite phase (∼0.5 μm). This indicated that it was the freshly transformed martensite that hindered crack growth, rather than its parent austenite phase. Such crack arresting worked for a prolonged period containing 11,001 cycles (from N_2 to N_4). During this period, the fatigue crack had remained stationary, and the actual crack extension was zero. When this interface barrier was finally overcome, fatigue crack growth resumed, and then an additional 4,001 cycles (from N_4 to N_5) were required for the martensite grain to be entirely penetrated by the crack. Due to this effect, the crack growth rate averaged over a predetermined crack extension can be dramatically reduced by one to two orders of magnitude, as shown in Fig. 2*E*. More examples of such a clear crack-arresting effect can be found in *SI Appendix*, Figs. S3 and S4. Interestingly, this phenomenon was not observed in the L-DIMT material with a low transformation tendency during the fatigue test. Hence, it reflects an essential difference between the H-DIMT material and the L-DIMT material in short fatigue crack growth behavior, and it allows explaining their significantly different crack growth rates of up to two orders of magnitude during Stage I. This cannot be explained by the existing DIMT-related mechanisms (involving TICC, TIEA, TICD, and RICC), because the effectiveness of all these mechanisms essentially depends on

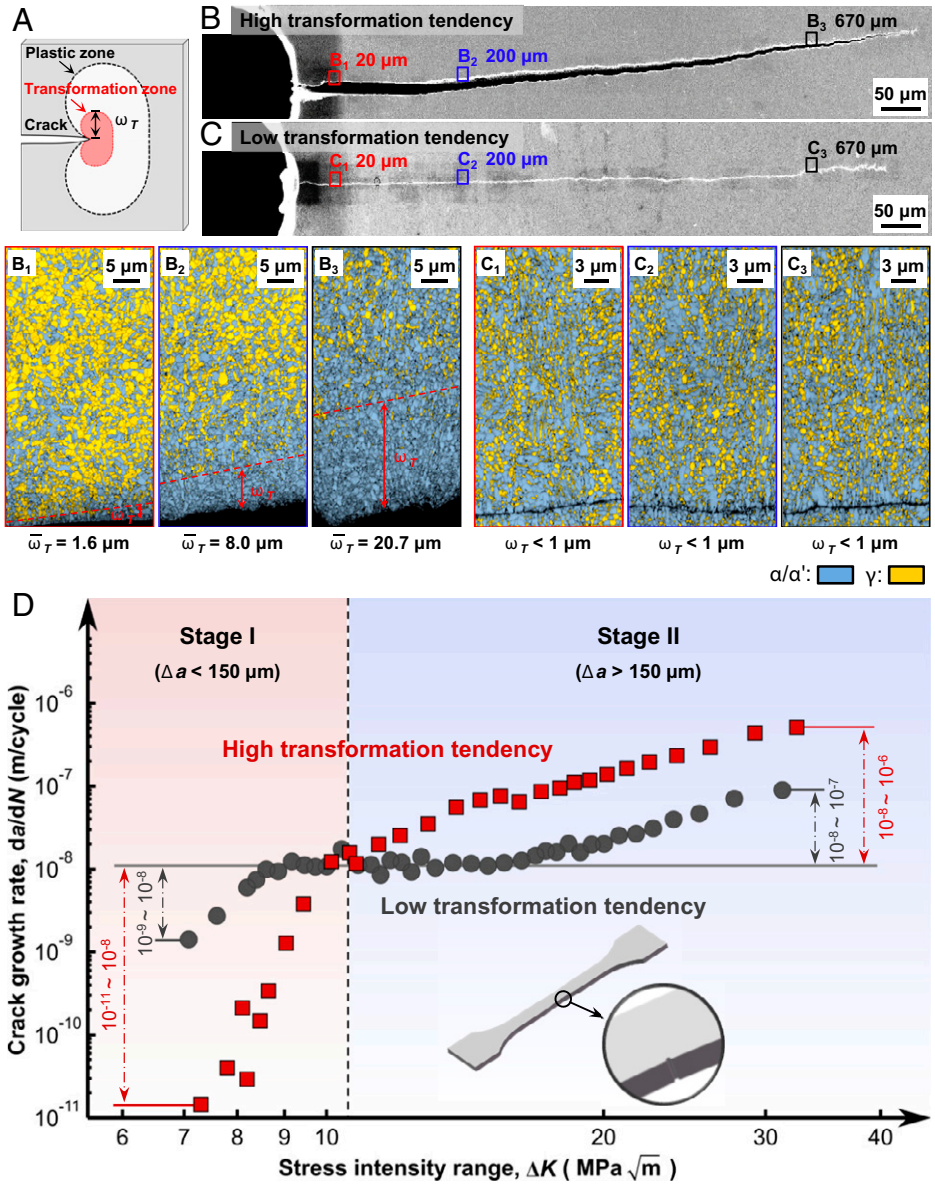

Fig. 1. Influence of DIMT on macroscopic fatigue crack growth behavior. (*A*) Schematic presentation of the phase transformation zone formed within the plastic zone ahead of a fatigue crack tip. (*B*) Secondary electron (SE) overview image showing the crack path in the H-DIMT sample with high transformation tendency after the fatigue test. (B_1–B_3) EBSD phase plus image quality (IQ) maps showing the microstructures in the areas corresponding to different crack extensions marked in *B*. The symbols of α, α′, and γ represent the phases of ferrite, martensite, and austenite, respectively. (*C*) SE overview image showing the crack path in the L-DIMT sample with low transformation tendency after the fatigue test. (C_1–C_3) EBSD phase plus IQ maps showing the microstructures in the areas corresponding to different crack extensions marked in *C*. (*D*) FCGRs. Crack growth rates *da*/*dN* as a function of applied stress intensity Δ*K*, measured for materials with high tendency (referred to as H-DIMT, marked with red squares) and low tendency (referred to as L-DIMT, marked with black filled circles), respectively, to undergo austenite-to-martensite transformation during deformation at room temperature. The geometric dimensions of the fatigue test samples are shown in *SI Appendix*, Fig. S2.

the amount of martensitic transformation, which is, however, limited in the short crack regime due to the small transformation zone formed near the crack tip. It can also not be explained by crack closure mechanisms other than DIMT, because the L-DIMT material consistently exhibits a closure stress level comparable to that of the H-DIMT material throughout the fatigue crack growth process from Stage I to Stage II (*SI Appendix*, Fig. S5). The underlying mechanisms of this fatigue crack arresting effect are elucidated in *Discussion*.

Fatigue Crack Coalescence at Stage II. When the fatigue crack growth in the H-DIMT material entered Stage II, the near-tip martensitic transformation zone expanded significantly (Fig. 1*B*), and some new microstructural features associated with the crack growth emerged. First, the above crack-arresting phenomenon can no longer be observed. More specifically, when the crack tip encountered an α′-martensite phase boundary it either passed through it directly (intragranular fracture) or bypassed it along the phase boundary (intergranular fracture), but in neither case did the crack show any noticeable stagnation. This is reflected by a smoother course of the crack growth rate curve in Stage II, without exhibiting the characteristic sharp drops related to the crack-arresting events observed before (*SI Appendix*, Fig. S6). Instead, another phenomenon was frequently observed in this long crack regime. This was the formation of secondary cracks in the near-tip field, as shown in Fig. 3. Fig. 3 *A* and *B* exhibit that

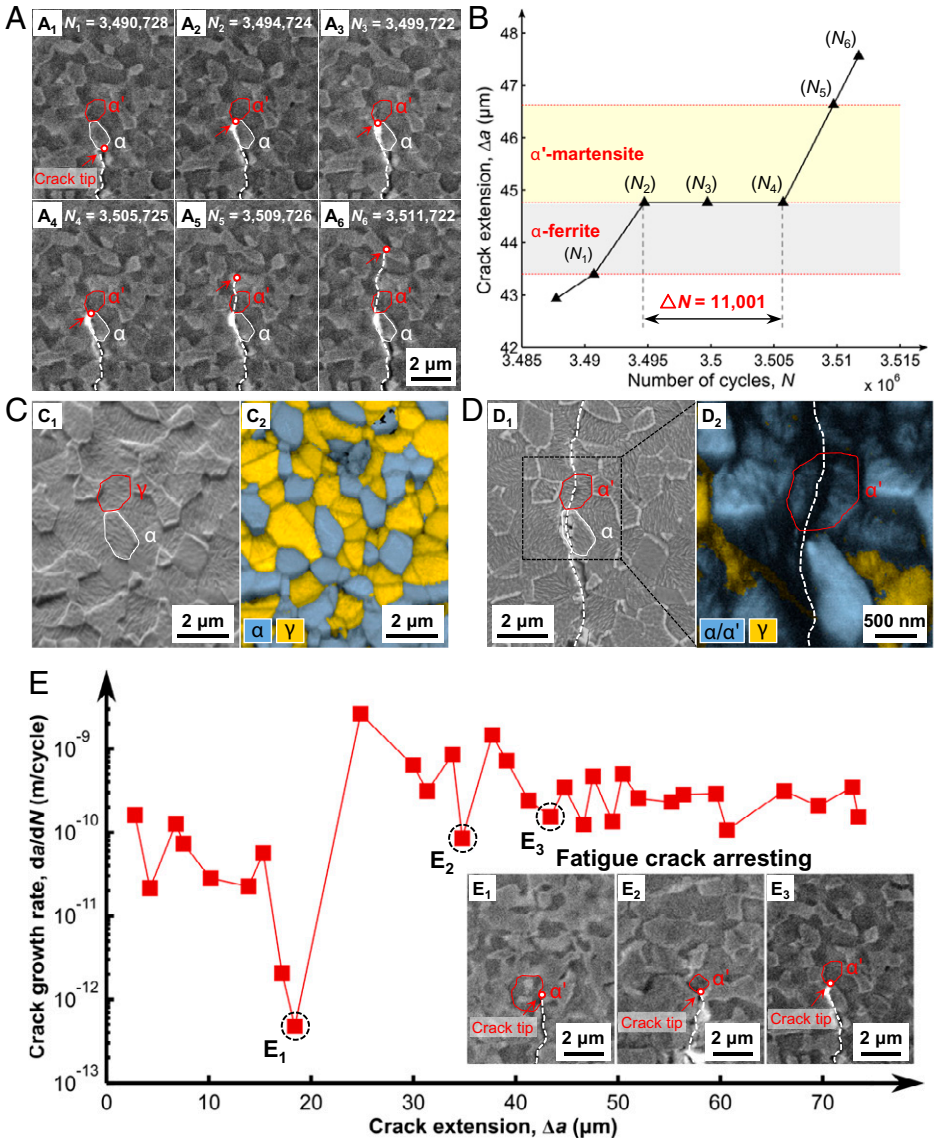

Fig. 2. Fatigue crack arresting. (*A*) A sequence of in situ SE images (A_1–A_6) probing the trajectory of the crack tip (marked with red open circles) in the region of interest (ROI) for crack extension Δ*a* from 43 μm to 47 μm at Stage I in the H-DIMT sample. The α-ferrite grain and α′-martensite grain involved are circled in white and red, respectively. (*B*) Fatigue crack extension Δ*a* as a function of the number of load cycles *N*. (*C*) Microstructure of the ROI in its initial undeformed state, where C_1 is an SE image of the ROI and C_2 is the corresponding EBSD phase plus IQ map. (*D*) Microstructure of the ROI after experiencing crack propagation in the entire zone, where D_1 is an SE image of the ROI and D_2 is the EBSD phase plus IQ map showing a close-up observation on a particularly relevant region in D_1 (marked with a dashed rectangle). (*E*) Influence of crack arresting on FCGR. Crack growth rates *da*/*dN* as a function of crack extension Δ*a* at Stage I in the H-DIMT sample. The points E_1–E_3 marked with dashed circles correspond to the moments of crack arresting events observed during the in situ fatigue test, as shown by *Insets*. Each of them corresponds to a sharp decrease in crack growth rate.

all the secondary cracks observed were located on both sides of the main crack, and their length varied from a few hundred nanometers to about 1 to 2 μm. It can be also confirmed that they were all formed within the near-tip transformation zone (that is larger than 8 μm at Stage II). Further analysis demonstrated that the secondary cracks formed either along ferrite–martensite (α–α′) interfaces (red dashed lines in Fig. 3 *C*–*F*) or inside α′-martensite grains (red solid lines in Fig. 3 *C*–*F*) due to DIMT. These secondary microcracks, formed in the near-tip region, tended to merge with the main crack. This created favorable conditions for crack extension through a crack coalescence process, as clearly shown in Fig. 3*C*. This effect accelerated fatigue crack growth, leading to a five to seven times higher FCGR compared with the L-DIMT material that did not show such an effect in Stage II (Fig. 1*D*). In this case, the DIMT plays a detrimental role in resisting fatigue crack growth. Here it is worth noting that this occurred under the condition that all other recognized fatigue-resisting mechanisms by DIMT (involving TICC, TIEA, TICD, and RICC) were still active and actually became more pronounced with an increasing fraction of martensitic transformation near the crack tip during Stage II. It thus strongly suggests that this adverse effect by crack coalescence is dominant in the long crack regime.

Discussion

The results presented above demonstrate two important fatigue phenomena in which DIMT plays a key role, namely, fatigue crack arresting in the short crack regime and fatigue crack

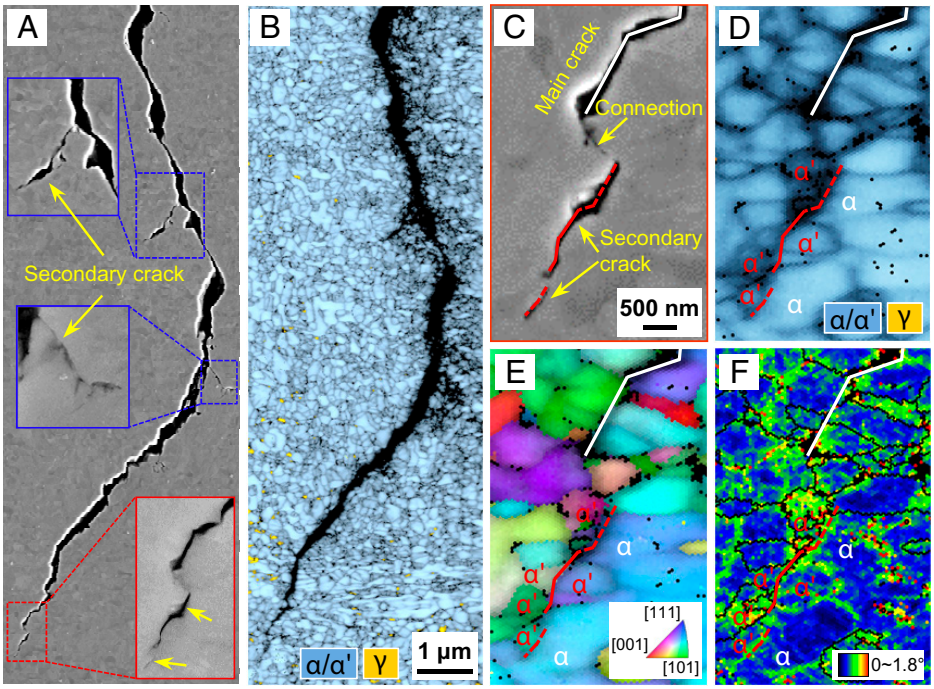

Fig. 3. Secondary crack formation. (*A*) SE image showing the front-end segment of a fatigue crack during Stage II in the H-DIMT sample, where *Insets* exhibit the presence of secondary cracks (pointed by yellow arrows) formed along the crack path. (*B*) EBSD phase plus IQ map corresponding to *A*. (*C*) SE image showing a close-up observation of the near-tip region of the fatigue crack in *A* (marked with a red rectangle). (*D–F*) EBSD phase plus IQ map, inverse pole figure, and kernel average misorientation map corresponding to *C*, respectively.

coalescence in the long crack regime. These two effects are schematically presented in Fig. 4, based on the in situ SEM observation results. Next, we discuss the underlying mechanisms of these two effects.

Mechanism of Fatigue Crack Arresting. The fatigue crack-arresting phenomenon observed in this work differs from the known fatigue-resisting mechanisms related to DIMT. First, the results have shown that the crack tip arresting occurs at the interface of α′-martensite at some point after the austenite-to-martensite transformation. Thus, the transformation process itself cannot be the direct cause of the crack arresting, so its related mechanisms, such as TIEA and TICD, are not applicable here. Second, the observed crack arresting shows an unusual discontinuity. It is characterized by a jump in crack growth rate occurring when the crack tip overcomes the interface barrier, and then the crack grows rapidly (~10^{-10} to 10^{-9} m per cycle)

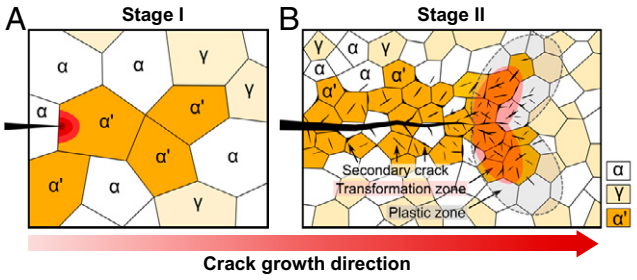

Fig. 4. Schematic illustration of fatigue crack growth with the presence of DIMT. (*A*) Fatigue crack growth in Stage I where the α′-martensite grain formed ahead of the crack tip acts as a strong microstructural barrier to crack growth, leading to abrupt and effective arresting of cracks. (*B*) Fatigue crack growth in Stage II where the secondary microcracks formed in the near-tip transformation zone lead to the acceleration of fatigue crack growth through a crack coalescence process.

inside the martensite grain (Fig. 2*E*). This occurs under considerable compressive residual stress within the martensite formed during the preceding DIMT process. Such an increase in crack growth rate cannot be attributed to the conventional crack closure mechanism (16, 17, 21). Hence, we propose a mechanism that relates the observed crack arresting to the characteristics of the fresh martensite formed at the crack tip as a transformation product. We refer to this mechanism as transformation-mediated crack arresting (TMCA) to emphasize the role of transformation only as a means to provide the necessary microstructure changes.

The nano-indentation tests show that the newly transformed martensite has excellent mechanical properties such as high hardness (*SI Appendix*, Fig. S7). We observed that the hardness of the transformed region in the vicinity of a crack tip can reach 7.8 GPa. This value is about 1.8 times the average hardness of the untransformed region (~4.4 GPa). This means that when the hard, fresh martensite appears as an obstacle along the path of an advancing crack passing through a soft ferrite grain, it acts as a strong mechanical barrier (as schematically shown in Fig. 4*A*). As a result, the crack tip is temporally arrested at the ferrite–martensite interface, and the fatigue crack growth stops. During this crack arresting, the dislocations emitted from the stressed crack tip will pile up at the interface, resulting in local stress concentration. This promotes the movement of dislocations in a small region of the forward martensite grain closest to the interface, leading to plastic strain localization. The local strain gradually accumulates under the cyclic fatigue loading until it reaches the failure tolerance of the material (i.e., the plastic strain at failure ε_f), and then local fracture occurs and the crack arresting is terminated. The ε_f of the present martensite was estimated to be 4.2% based on its carbon content (0.315 wt %, determined by atom probe tomography, APT) according to the literature (31). Then, the average plastic strain increment ($\Delta\varepsilon_p$) per cycle can be estimated to be 3.8 to 7.0 × 10^{-6} depending on the duration of the crack arresting (~6,000 to

11,000 cycles). This requires an increase in mobile dislocation density ($\Delta\rho_m$) of 1.8 to 3.2 × 10^{11} m^{-2} per cycle according to the following equation (32):

$$\Delta\varepsilon_p = \Delta\rho_m bL/M, \quad [1]$$

where b is the magnitude of the Burger vector [0.25 nm (33)], L is the average glide distance of the mobile dislocations (~250 nm), and M is the Taylor factor [2.9 (34)]. This dislocation multiplication occurs at a low local strain rate (~10^{-5} to 10^{-4} s^{-1}) during the fatigue test (5 Hz), and the preceding DIMT has already introduced a sufficient density of mobile dislocations within the martensite [enabling an initial value of ρ_m as high as 2 to 4 × 10^{15} m^{-2}, observed in a tensile test (35)]. These two factors provide favorable conditions for achieving the required dislocation multiplication during each cycle.

Mechanism of Fatigue Crack Coalescence. When an initially short fatigue crack (Stage I) grows into a long fatigue crack (Stage II), the crack growth behavior has undergone a fundamental change with the formation of a near-tip plastic zone. Its sensitivity to the specific crack tip microstructure is significantly reduced. Instead, it is predominantly controlled by the near-tip stress and strain fields on a larger scale (36). Then, the microstructure-sensitive TMCA mechanism is rendered less significant, and another mechanism mediated by the martensite transformation, the so-called transformation-mediated crack coalescence (TMCC), prevails. Here we utilized an SEM-based μ-DIC method to experimentally evaluate the near-tip strain field evolution of the H-DIMT sample (*SI Appendix*, Fig. S8). It shows that large-scale plastic deformation occurs near the crack tip, with an estimated plastic zone size ω_M (37) ranging from 189 μm to 543 μm in Stage II. The near-tip plastic zone promotes DIMT and the formation of a transformation zone with the size varying from 8 μm to 24 μm in Stage II. Since the formed fresh martensite is brittle (38, 39) (with an estimated plastic strain at failure of only 4.2%), local damage features are formed in the martensite grains or at the martensite interfaces under the repeated fatigue loading (18). The large plastic zone thus promotes the formation of a damage zone filled with secondary microcracks ahead of the main crack tip (as schematically shown in Fig. 4*B*). These microcracks coalesce with the main crack, accelerating crack growth. This means that this fatigue acceleration mechanism of TMCC is in essence due to the brittle character of the martensite as a transformation product. Here we ruled out the possible effect of element segregation on microcrack formation by performing APT characterization. The result shows that there is no detrimental element segregation at the ferrite–austenite phase boundaries, as shown in *SI Appendix*, Fig. S9. This confirms that the two fatigue mechanisms identified in this work, i.e., TMCA and TMCC, are due to the inherent dual characteristics of the formed martensite phase from DIMT, namely, hard and brittle. Their crack size dependence is essentially due to the transition of the governing fatigue mechanism at the crack tip when the crack driving force increases with the crack length. This transition from the TMCA mechanism to the TMCC mechanism is reflected in the change in fracture characteristics when the crack propagates from Stage I to Stage II, as shown in *SI Appendix*, Fig. S10. The crack environment exhibits predominantly ductile features in Stage I due to the sustained cyclic plastic straining associated with the TMCA mechanism. By comparison, the fracture surfaces in Stage II show more brittle features with the emergence of many intergranular facets produced during the TMCC process.

To conclude, the present study reveals the dual role of DIMT in fatigue crack growth. Two transformation-mediated fatigue mechanisms, namely, TMCA and TMCC, have been identified, and their crack size dependence can be consistently interpreted. These insights help to clarify the role of martensitic transformation in fatigue and resolve some of the contradictions in the literature, by illuminating both its beneficial and adverse micromechanical effects and underlying mechanisms. The observations may also assist in developing microstructure-based lifetime models for metastable alloys that are exposed to fatigue loads. Furthermore, it opens up new avenues for the use of martensitic transformation to design advanced alloys with fatigue-resistant microstructures. A promising path for that might be to design microstructures with chemical gradients that create alternating regions of variable austenite stability. This would lead to likewise alternating transformation patterns that could effectively block fatigue crack growth.

Materials and Methods

Material Preparation. The two microstructure variants used in this work, namely, the H-DIMT material and the L-DIMT material, were obtained from the same base material, i.e., a medium-Mn steel composed of 0.2C-10.2Mn-2.8Al-1Si (in wt %). The material with H-DIMT microstructure was prepared by applying an intercritical annealing temperature of 800 °C for 10 min in a box furnace, followed by water quenching. It led to a relatively low content of C and Mn partitioned into austenite (0.23 wt % C and 10.6 wt % Mn, calculated by the Thermo-Calc software using the TCFE 7 database), and therefore a low austenite stability ($|\Delta G_{\gamma\rightarrow\alpha'}|$ = 3,650 J/mol at room temperature). In contrast, the material with L-DIMT microstructure was prepared under a lower intercritical annealing temperature of 700 °C while the other conditions remained unchanged. This treatment led to enrichment of C and Mn within the austenite (0.33 wt % C and 13.0 wt % Mn; *SI Appendix*, Fig. S1*A*), and thus to a high austenite stability ($|\Delta G_{\gamma\rightarrow\alpha'}|$ = 3,276 J/mol at room temperature). The microstructures, tensile test properties, and transformation kinetics of the two materials are illustrated in *SI Appendix*, Fig. S1 *B–G* , and more details can be found in our previous study (40).

Fatigue Testing. A single-edge-notched plate sample was adopted for FCGR testing, as shown in *SI Appendix*, Fig. S2. A sharp precrack of 30 μm was prepared by cyclic loading at the notch with a radius of 100 μm and a depth of 100 μm. We used moderate loads and prolonged testing time to carefully control the precracking process to minimize any additional plasticity or microstructural effects introduced near the notch that may affect the subsequent fatigue crack growth. This was confirmed by EBSD measurements in the region near the precrack tip (*SI Appendix*, Fig. S11). The conventional ΔK-increasing FCGR (*da/dN*) testing was then performed on the precracked samples using an SEM built-in fatigue testing system Shimadzu SEM-Servo Pulser. It enabled in situ observation of crack growth and microstructural evolution of the sample surface during the fatigue process. The constant-amplitude fatigue tests were conducted with an applied stress ratio of 0.1 and a load frequency of 5 Hz at room temperature. The nominal stress range $\Delta\sigma_n$ was limited to about 25 to 40% of the yield strength of the material to realize high-cycle fatigue loading conditions (~10^4 to 10^7 cycles to failure). The nominal stress intensity range ΔK was used as a measure of the crack driving force in this work, as it can consider both the nominal stress range $\Delta\sigma_n$ and the crack length a, the two key external conditions for controlling fatigue crack growth. The applied ΔK varied from 7 MPa $m^{1/2}$ to 34 MPa $m^{1/2}$ during the fatigue tests. It allowed a sufficiently wide range of *da/dN* to be covered, from 10^{-11} m per cycle to 10^{-6} m per cycle. During the fatigue crack propagation, the crack length a was recorded in real time using in situ SEM imaging. The average *da/dN* was then evaluated over a certain crack extension. The fatigue testing was halted when the initially microcrack grew into a macrocrack with a length about 1 mm. More details on the assessment of *da/dN*-ΔK data are presented in *SI Appendix*. Moreover, an SEM-based μ-DIC method (41) was applied to quantify the near-tip plastic zone and monitor its evolution in situ. It was also used to estimate the crack closure stress σ_{cl} according to the established procedure in ref. 42.

Microstructure Characterization. In addition to the in situ fatigue testing, ex situ microstructural characterization on the test samples were also conducted. The fatigue cracks and fracture surfaces were characterized by SE imaging (Zeiss-Sigma and Zeiss-Merlin SEM). The microstructures surrounding the fatigue cracks were probed by EBSD (JEOL JSM-6500F and Zeiss-Sigma SEM). The acquired EBSD data (phase, fraction, orientation, and misorientation) were analyzed using the TSL OIM software package. The differentiation of α-ferrite from α′-martensite was based on the intensity of the image quality

map signal and the kernel average misorientation, both of which were proven to be effective methods due to the high defect content in α′-martensite (38, 43). Nano-indentation testing was applied to quantify the hardening effect both in the areas close to and away from the fatigue crack tips. The tests were performed by a Bruker Hysitron TriboScope, using a Berkovich shaped indenter with a load of 2,000 μN. APT characterization was carried out using a LEAP 5000X HR instrument (Cameca Instruments Inc.) equipped with a reflection lens. Site-specific APT tips were prepared using a dual beam SEM/focused-ion-beam instrument (FEI Helios Nanolab 600i). APT experiments were conducted in a laser pulse mode with a pulse rate of 200 kHz, pulse energy of 40 pJ, sample temperature of 60 K, and detection rate of 15 ions per 1,000 pulses. The analysis of the APT data was performed using the IVAS 3.8.4 software.

Data Availability. All study data are included in the article and/or *SI Appendix*.

ACKNOWLEDGMENTS. X.W. and C.J. acknowledge the financial support from the National Natural Science Foundation of China (Grants 51975195 and 51725502). B.S. acknowledges the research fellowship provided by the Alexander von Humboldt Foundation.

1. G. Olson, M. Cohen, Kinetics of strain-induced martensitic nucleation. *Metall. Trans., A, Phys. Metall. Mater. Sci.* **6**, 791 (1975).
2. H. Bhadeshia, R. Honeycombe, *Steels: Microstructure and Properties* (Butterworth-Heinemann, 2017).
3. P. Jacques, Transformation-induced plasticity for high strength formable steels. *Curr. Opin. Solid State Mater. Sci.* **8**, 259–265 (2004).
4. O. Matsumura, Y. Sakuma, H. Takechi, Trip and its kinetic aspects in austempered 0.4C-1.5Si-0.8Mn steel. *Scr. Metall.* **21**, 1301–1306 (1987).
5. R. O. Ritchie, The conflicts between strength and toughness. *Nat. Mater.* **10**, 817–822 (2011).
6. P. Gibbs *et al.*, Austenite stability effects on tensile behavior of manganese-enriched-austenite transformation-induced plasticity steel. *Metall. Mater. Trans., A Phys. Metall. Mater. Sci.* **42**, 3691–3702 (2011).
7. B. B. He *et al.*, High dislocation density-induced large ductility in deformed and partitioned steels. *Science* **357**, 1029–1032 (2017).
8. M. Marteleur *et al.*, On the design of new β-metastable titanium alloys with improved work hardening rate thanks to simultaneous TRIP and TWIP effects. *Scr. Mater.* **66**, 749–752 (2012).
9. Z. Li, K. G. Pradeep, Y. Deng, D. Raabe, C. C. Tasan, Metastable high-entropy dual-phase alloys overcome the strength-ductility trade-off. *Nature* **534**, 227–230 (2016).
10. S. Suresh, *Fatigue of Materials* (Cambridge University Press, 1998).
11. Y. Murakami, Material defects as the basis of fatigue design. *Int. J. Fatigue* **41**, 2–10 (2012).
12. L. L. Li, Z. J. Zhang, P. Zhang, Z. G. Wang, Z. F. Zhang, Controllable fatigue cracking mechanisms of copper bicrystals with a coherent twin boundary. *Nat. Commun.* **5**, 3536 (2014).
13. A. Pineau, R. Pelloux, Influence of strain-induced martensitic transformations on fatigue crack growth rates in stainless steels. *Metall. Trans.* **5**, 1103–1112 (1974).
14. D. Martelo, A. Mateo, M. Chapetti, Crack closure and fatigue crack growth near threshold of a metastable austenitic stainless steel. *Int. J. Fatigue* **77**, 64–77 (2015).
15. M. Koyama *et al.*, Bone-like crack resistance in hierarchical metastable nanolaminate steels. *Science* **355**, 1055–1057 (2017).
16. H. Mayer, S. Stanzl-Tschegg, Y. Sawaki, M. Hühner, E. Hornbogen, Influence of transformation-induced crack closure on slow fatigue crack growth under variable amplitude loading. *Fatigue Fract. Eng. Mater. Struct.* **18**, 935–948 (1995).
17. W. Elber, "The significance of fatigue crack closure" in *Damage Tolerance in Aircraft Structures*, M. S. Rosenfeld, Ed. (ASTM International, 1971), pp. 230–242.
18. E. Hornbogen, Martensitic transformation at a propagating crack. *Acta Metall.* **26**, 147–152 (1978).
19. R. McMeeking, A. Evans, Mechanics of transformation-toughening in brittle materials. *J. Am. Ceram. Soc.* **65**, 242–246 (1982).
20. B. Budiansky, J. Hutchinson, J. Lambropoulos, Continuum theory of dilatant transformation toughening in ceramics. *Int. J. Solids Struct.* **19**, 337–355 (1983).
21. Z. Mei, J. Morris, Influence of deformation-induced martensite on fatigue crack propagation in 304-type steels. *Metall. Trans., A, Phys. Metall. Mater. Sci.* **21**, 3137–3152 (1990).
22. S. D. Antolovich, B. Singh, On the toughness increment associated with the austenite to martensite phase transformation in TRIP steels. *Metall. Mater. Trans., B, Process Metall. Mater. Proc. Sci.* **2**, 2135–2141 (1971).
23. X. Cheng, R. Petrov, L. Zhao, M. Janssen, Fatigue crack growth in TRIP steel under positive R-ratios. *Eng. Fract. Mech.* **75**, 739–749 (2008).
24. M. Song *et al.*, Transformation induced crack deflection in a metastable titanium alloy and implications on transformation toughening. *Acta Mater.* **118**, 120–128 (2016).
25. Y.-B. Ju, M. Koyama, T. Sawaguchi, K. Tsuzaki, H. Noguchi, In situ microscopic observations of low-cycle fatigue-crack propagation in high-Mn austenitic alloys with deformation-induced ε-martensitic transformation. *Acta Mater.* **112**, 326–336 (2016).
26. S. Suresh, Crack deflection: Implications for the growth of long and short fatigue cracks. *Metall. Trans., A, Phys. Metall. Mater. Sci.* **14**, 2375–2385 (1983).
27. S. Suresh, R. Ritchie, A geometric model for fatigue crack closure induced by fracture surface roughness. *Metall. Trans., A, Phys. Metall. Mater. Sci.* **13**, 1627–1631 (1982).
28. G. Baudry, A. Pineau, Influence of strain-induced martensitic transformation on the low-cycle fatigue behavior of a stainless steel. *Mater. Sci. Eng.* **28**, 229–242 (1977).
29. T. Niendorf *et al.*, Fatigue crack growth–Microstructure relationships in a high-manganese austenitic TWIP steel. *Mater. Sci. Eng. A* **527**, 2412–2417 (2010).
30. K. Tsuzaki, E. Nakanishi, T. Maki, I. Tamura, Low-cycle fatigue behavior in metastable austenitic steel accompanying deformation-induced martensitic transformation. *Trans. Iron Steel Inst. Jpn.* **23**, 834–841 (1983).
31. G. Krauss, Martensite in steel: Strength and structure. *Mater. Sci. Eng. A* **273**, 40–57 (1999).
32. J. Hirth, J. Lothe, *Theory of Dislocations* (John Wiley & Sons, 1982).
33. D. Akama, T. Tsuchiyama, S. Takaki, Change in dislocation characteristics with cold working in ultralow-carbon martensitic steel. *ISIJ Int.* **56**, 1675–1680 (2016).
34. M. Sauzay, B. Fournier, M. Mottot, A. Pineau, I. Monnet, Cyclic softening of martensitic steels at high temperature—Experiments and physically based modelling. *Mater. Sci. Eng. A* **483**, 410–414 (2008).
35. F. Christien, M. Telling, K. Knight, Neutron diffraction in situ monitoring of the dislocation density during martensitic transformation in a stainless steel. *Scr. Mater.* **68**, 506–509 (2013).
36. D. S. Dugdale, Yielding of steel sheets containing slits. *J. Mech. Phys. Solids* **8**, 100–104 (1960).
37. T. L. Anderson, *Fracture Mechanics: Fundamentals and Applications* (CRC Press, 2017).
38. B. Sun *et al.*, Revealing fracture mechanisms of medium manganese steels with and without delta-ferrite. *Acta Mater.* **164**, 683–696 (2019).
39. C. C. Tasan *et al.*, An overview of dual-phase steels: Advances in microstructure-oriented processing and micromechanically guided design. *Annu. Rev. Mater. Res.* **45**, 391–431 (2015).
40. B. Sun *et al.*, Improving the ductility of ultrahigh-strength medium Mn steels via introducing pre-existed austenite acting as a "reservoir" for Mn atoms. *Mater. Sci. Eng. A* **749**, 235–240 (2019).
41. X. Wang, C. Liu, B. He, C. Jiang, M. Huang, Microscopic strain partitioning in Lüders band of an ultrafine-grained medium Mn steel. *Mater. Sci. Eng. A* **761**, 138050 (2019).
42. M. A. Sutton *et al.*, "Local crack closure measurements: Development of a measurement system using computer vision and a far-field microscope" in *Advances in Fatigue Crack Closure Measurement and Analysis*, R. C. McClung, J. C. Newman, Eds. (ASTM International, 1999), vol. 2, pp. 145–156.
43. B. Sun, W. Krieger, M. Rohwerder, D. Ponge, D. Raabe, Dependence of hydrogen embrittlement mechanisms on microstructure-driven hydrogen distribution in medium Mn steels. *Acta Mater.* **183**, 313–328 (2020).